Applied Energy 317 (2022) 119155

Contents lists available at ScienceDirect

Applied Energy

journal homepage: www.elsevier.com/locate/apenergy

A holistic methodology for hydrokinetic energy site selection

D.M. Fouz [a], R. Carballo [a,*], I. López [a], G. Iglesias [b,c]

[a] Departamento de Enxeñaría Agroforestal, Universidade de Santiago de Compostela, EPSE, Rúa Benigno Ledo s/n, 27002 Lugo, Spain
[b] School of Engineering and Architecture & MaREI, Environmental Research Institute, University College Cork, Ireland
[c] School of Engineering, Computing and Mathematics, University of Plymouth, UK

HIGHLIGHTS

- A holistic methodology for hydrokinetic energy exploitation site selection is proposed.
- The novel Integrated Hydrokinetic Energy (IHE) index is developed.
- The IHE index is applied to the Shannon Estuary.
- The optimum areas for hydrokinetic energy exploitation are identified.

ARTICLE INFO

Keywords:
Hydrokinetic energy
Tidal power
Numerical modelling
Socioeconomic impact
CAPEX

ABSTRACT

Hydrokinetic energy can contribute to diversify and decarbonise the energy mix in many coastal regions, in particular estuaries. These are typically areas of high environmental value and with intense socioeconomic activity. The aim of this work is to provide a comprehensive methodology for selecting the optimum locations for hydrokinetic energy exploitation, by considering all the relevant aspects which affect the decision-making process, and improve the current available procedures. The methodology is centred around a novel holistic index, the Integrated Hydrokinetic Energy (IHE) index, which considers: (i) the exploitable resource, (ii) the costs of installation, and (iii) the socioeconomic and environmental aspects. The approach is illustrated through a case study in the Shannon Estuary, on the west coast of Ireland. It is shown that the application of this methodology facilitates the planning and reduces the uncertainties in the development of a hydrokinetic farm project.

1. Introduction

Marine renewable energies (MREs) have been recognised as a significant source of green energy, with potential to contribute to reducing greenhouse gases emissions and thus combat climate change [1–4]. Within MREs, hydropower is highlighted as a feasible alternative renewable energy source, which may be used to diversify and decarbonise the energy mix in many regions [5–9]. Focusing on coastal areas, a specific type of hydropower, hydrokinetic energy, stands out because of its predictability, electricity quality and low environmental impact [10–12]. In this regard, estuaries are promising areas for the exploitation of hydrokinetic energy thanks to their strong tidal currents and, in some cases, large fluvial discharges [13–15], or sea level rise [16].

Over the last years, considerable efforts have been made to develop hydrokinetic energy converters (HECs), with emphasis on hydrokinetic turbines [17,18], and to identify the best areas for their operation [10,14,19–25]. For all their interest, these studies were carried out from the perspective of the energy yield, disregarding economic and environmental aspects; therefore, more comprehensive studies are required for an informed decision–making process in developing a hydrokinetic farm project [26]. This is of great importance in the case of estuaries, where different areas for installing HECs may be of interest. In effect, the costs of installation and operation of a hydrokinetic farm, along with the restrictions that would be imposed by the existing or potential socioeconomic activities and environmental aspects, may greatly differ among locations within the same coastal area [27].

In this research, a novel comprehensive methodology is developed for selecting the most suitable location for hydrokinetic energy exploitation in a coastal region, irrespective of the conversion technology or farm layout, and therefore significantly improving the current available procedures, by considering the key aspects affecting the decision-making process. The application of this methodology to a coastal

* Corresponding author.
E-mail address: rodrigo.carballo@usc.es (R. Carballo).

https://doi.org/10.1016/j.apenergy.2022.119155
Received 10 February 2022; Received in revised form 1 April 2022; Accepted 15 April 2022
Available online 25 April 2022
0306-2619/© 2022 The Authors. Published by Elsevier Ltd. This is an open access article under the CC BY license (http://creativecommons.org/licenses/by/4.0/).

region will allow the reduction of the uncertainties in the early stages of planning the installation of a hydrokinetic farm [28]. The final design of the farm configuration in subsequent stages would require a detailed cost analysis [29,30].

The proposed integrated site selection is conducted by means of the novel Integrated Hydrokinetic Energy (IHE) index. Based on a holistic approach, the IHE index integrates the three main aspects affecting the installation of hydrokinetic energy farms: (i) the exploitable resource, which is computed by high–resolution numerical modelling; (ii) the geomorphological configuration, for which the main Capital Expenditures (CAPEX) of a hydrokinetic farm are parameterised according to water depth and shoreline distance; (iii) the socioeconomic activities (aquaculture, shellfish, and shipping) and environmental uses (Special Areas of Conservation, SACs, Spatial Protection Areas, SPAs) which are considered by analysing and parameterising a large amount of geospatial data.

In this work, the IHE index is defined and applied to a case study: the Shannon Estuary, on the west coast of Ireland (Fig. 1). The Shannon Estuary is a macrotidal coastal area characterised, from a hydrodynamic perspective, by a semidiurnal tidal regime and large riverine inputs from several tributaries subject to a marked seasonality. A number of areas of interest for hydrokinetic energy conversion were identified in preliminary studies, in particular the Strategic Integrated Framework Plan for the Shannon Estuary (SIFP) [31]. Likewise, in recent studies based on the Tidal Stream Exploitability index adapted to non-depth-limited areas, TSE_{ndl} index, a number of areas were identified as of potential interest [13]: Kilcredaun (Area I), the constriction between Scattery Island and Carrig Island (Area II), the area close to Moneypoint (Area III), Tarbert (Area IV), the surroundings of Glin (Area V), the approaches to Port of Foynes (area VI), the area close to Aughinish (Area VII). However, a comprehensive analysis of these areas encompassing not only the resource itself but also the socioeconomic and environmental aspects is lacking to the best of the authors' knowledge.

Regarding its geomorphologic configuration, the Shannon Estuary has extensive deep (over 20 m) areas (main channel), areas of intermediate water depths, and intertidal areas. The average water depth is approximately 16 m. With much of its area sheltered from wave action and a wide and deep main channel, the Shannon Estuary is an excellent location for a port. Indeed, with its six commercial maritime terminals, the Shannon Foynes port is the second largest in Ireland, after Dublin, in terms of commercial traffic. These activities must naturally be accounted for in developing hydrokinetic energy. More generally, a thorough investigation of the costs, socioeconomic activity and environmental aspects of the areas of interest is required for the definition of a plan for developing hydrokinetic energy in the Shannon Estuary.

This paper is structured as follows. In Section 2, a general overview of the IHE index is presented. Next, in Sections 3 to 5, the different aspects considered in the index are defined: the energy resource (Section 3), costs (Section 4), and socioeconomic and environmental uses (Section 5). In Section 6, the results are presented. Finally, conclusions are drawn in Section 7.

2. General description of the procedure

The objective of this research is to define and apply a comprehensive methodology, leading to the identification of the most suitable area for hydrokinetic energy exploitation in a coastal region, independently of the type of energy converter or farm layout. To this end, the IHE index is developed, based on a holistic procedure, while considering: (i) the exploitable resource, (ii) the costs of installation and operation, and (iii) the socioeconomic and environmental activities.

This procedure is carried out by considering four different steps: (i) a thorough characterisation of the energy resource, based on high–resolution spatiotemporal numerical modelling, (Section 3); (ii) the development of a geospatial penalty function while considering the relation between the main drivers of the CAPEX and the coastal configuration (depth and distance to coast), leading to a penalisation of those areas where the costs of hydrokinetic energy exploitation are higher (Section 4); (iii) an accurate geospatial analysis of socioeconomic and environmental uses, assessing the suitability of their coexistence with hydrokinetic energy exploitation, leading to an additional penalty function (Section 5); and finally, (iv) the integration of previous results (i to iii) in order to provide a reliable indicator that shows the viability of the hydrokinetic energy exploitation throughout a coastal region (Section 6).

Each one of the aforementioned steps is reflected in the corresponding term that constitutes the IHE index, which is computed as follows:

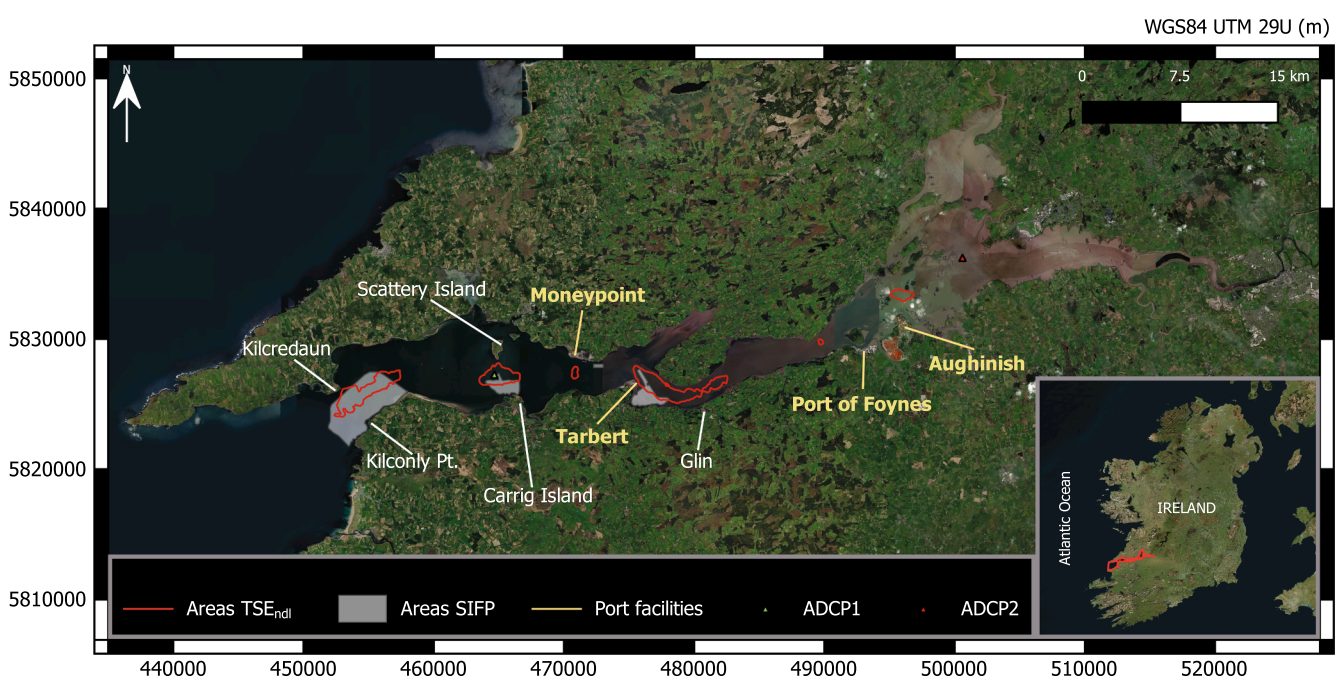

Fig. 1. Location of the Shannon Estuary.

$$\mathrm{IHE} = \mathrm{HE} C_{gp} U_{gp}, \tag{1}$$

where HE is the hydrokinetic energy resource index (step i), according to which values equal to or higher than 1 indicate suitability for energy exploitation; C_{gp} is a geospatial cost penalty function (values ranging from 1 to 0) (step ii), meaning that a location with $C_{gp} = 1$ is not penalised by the costs that are associated to the operation and maintenance of a hydrokinetic farm, and where $C_{gp} = 0$ has the largest penalisation (in the latter case, IHE = 0); finally, U_{gp} stands for the geospatial water use penalty function (values ranging from 0 to 1) (step iii), having the same interpretation as C_{gp}. As a result, the physical interpretation of the IHE index is straightforward. The higher the IHE index, the better the site for hydrokinetic energy exploitation, with values above 1 indicating suitability for hydrokinetic energy exploitation, which would correspond with a site with IHE = 1 (minimum value for suitability), and without any penalisation ($C_{gp} = 1$ and $U_{gp} = 1$).

3. Hydrokinetic energy resource (HE) index

The first step of the proposed methodology is to define an index which accurately reflects the suitability of a given coastal area, by considering not only its total available energy, but its exploitable resource. To this end, the hydrokinetic energy (HE) resource index is defined as:

$$\mathrm{HE} = \frac{E_e}{E_{ref}}, \tag{2}$$

where E_e is the exploitable energy resource at a given location, i.e., the resource resulting from current velocity magnitudes that allow a tidal turbine to operate (Section 3.2), and E_{ref} is a reference level of energy resource representing the minimum annual energy that is required for hydrokinetic energy exploitation. In the following subsections the development of HE is presented, along with its application to the Shannon Estuary.

3.1. Numerical modelling

An accurate characterisation of the hydrokinetic energy potential in a coastal region, requires a thorough description of its hydrodynamics during a long period of time, ideally a complete year [19], for which high-resolution spatiotemporal numerical modelling constitutes a powerful tool [32]. To this end, the state-of-the-art model Delft3D-FLOW is applied, which has been widely used to analyse the hydrodynamics of estuarine areas [33–38]. This model approximates the Navier–Stokes equations under the Shallow Water and Boussinesq's assumptions by means of a finite–difference scheme. The results are coupled with the transport equation (in terms of water temperature and salinity), leading to the computation of the density spatial distribution and thus the baroclinic flows, which in turn may be of importance in coastal areas that are subject to large river discharges, or where two different types of water masses meet [39,40]. The Delft3D–FLOW model can be implemented in its 3D or 2DH form (i.e., vertically averaged). The usual dominance of the tide in the coastal areas of interest for hydrokinetic energy exploitation leads to 2DH models, being those that are most used in energy resource assessments [10,13,14,32,41]. For further details about the Delft3D–FLOW model, the reader is referred to [42].

In the present work, a high-resolution 2DH application of the Delft3D–FLOW model is conducted for the Shannon Estuary and the adjacent continental shelf, up to 100 m water depth, approximately. To this end, a varying–size numerical grid (Fig. 2) is used, covering the whole estuary and extending over the Atlantic Ocean, approximately 30 km offshore. From the inner estuary to the mouth, the grid resolution is set to 100 × 100 m, progressively decreasing up to 100 × 300 m, towards the westernmost oceanic open boundary. The bathymetric data is obtained from the INFOMAR programme (Integrated Mapping for the Sustainable Development of Ireland's Marine Resource) [43]. The numerical model is validated against ADCP (Acoustic Doppler Current Profiler) field measurements of flow velocity, gathered at two different locations in the inner and middle estuary (Fig. 1), ADCP1 (25/06/2017 to 29/07/2017) and ADCP2 (24/03/2006 to 28/03/2006). Fig. 3 shows the linear regression fit of the magnitude of computed and observed velocities at ADCP1 and ADCP2, and Table 1 provides the statistical parameters obtained. The results show an excellent agreement between both time series, and, therefore, the capability of the model to accurately reproduce the hydrodynamics of this coastal area.

Once the numerical model is validated, it can be used to accurately characterise the available energy resource. With this aim, a complete annual scenario is computed by using the following forcing factors: main tidal harmonics (TOPEX/Poseidon database) [44,45], average monthly river discharges (Irish Office of Public Works, OPW), and thermohaline conditions at open boundaries (Irish Marine Institute, MI).

3.2. Available and exploitable energy resource

The available time-dependent hydrokinetic energy resource is computed in terms of power density, $E_a(t)$ (Wm^{-2}), as [10]:

$$E_a(t) = \frac{\rho}{2}[V(t)]^3, \tag{3}$$

where ρ (kgm^{-3}) is the seawater density and $V(t)$ (ms^{-1}) stands for the time–dependent flow velocity. In Fig. 4 the spatial distribution of the mean flow velocity, V_m, during a complete annual scenario is plotted.

However, all of the available resource cannot be harnessed. In effect, HECs usually work within a range of velocities, defined by lower and upper thresholds [41]: the so–called cut-in velocity, V_{ci} (ms^{-1}), which indicates the minimum velocity that is required for their operation, and the cut-off velocity, V_{co} (ms^{-1}), or the maximum velocity at which HECs can operate, due to safety reasons.

In view of the aforementioned aspects, the exploitable time-dependent energy resource in terms of power density, $E_e(t)$ (Wm^{-2}) is

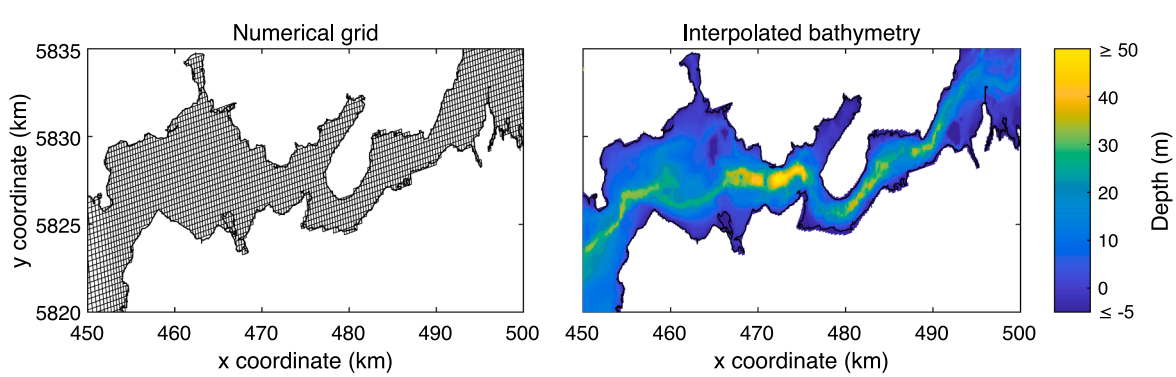

Fig. 2. Numerical grid (left) and its interpolation to the bathymetric data (right).

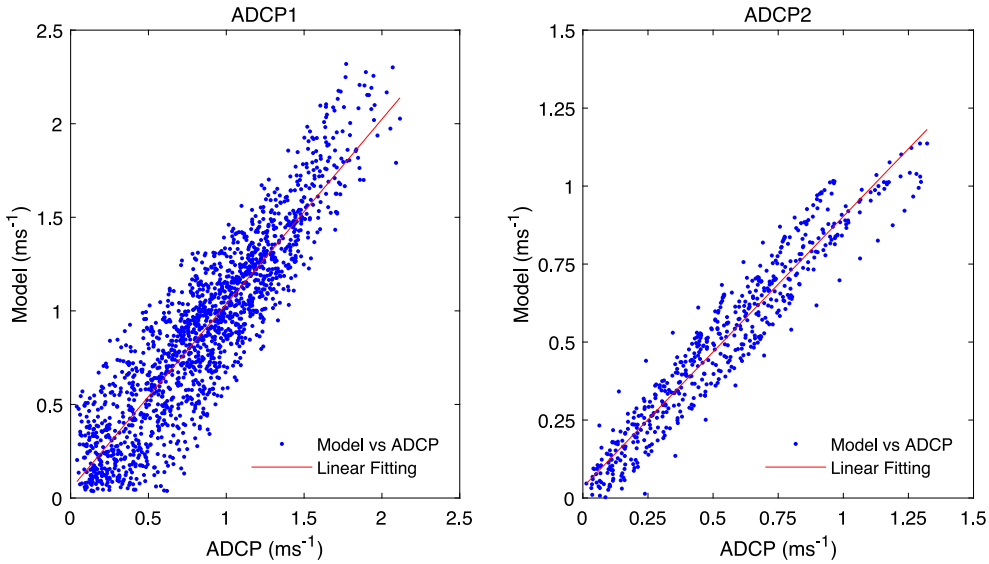

Fig. 3. Numerical model validation against ADCP measurements at ADCP1 (left) and ADCP2 (right) sites.

Table 1
Validation: statistical parameters.

Parameter	ADCP1	ADCP2
R	0.900	0.959
NRMSE (%)	10.162	6.038
BIAS (ms^{-1})	0.038	−0.037
SI	0.245	0.146

defined as [41]:

$$E_e(t) = \begin{cases} 0, V(t) < V_{ci} \\ \frac{\rho}{2}[V(t)]^3, V_{ci} \le V(t) \langle V_{co} \\ 0, V(t) \ge V_{co} \end{cases}, \quad (4)$$

and therefore the mean non-exploitable power density, E_{ne} (Wm^{-2}) can be computed as:

$$E_{ne} = E_a - E_e \quad (5)$$

where E_a and E_e are the mean available and mean exploitable power density, respectively, over a given period of interest.

As previously stated, the objective of this work is to provide a methodology, which can be applied with independence of the energy conversion technology and farm layout. Thus, in the present application, and on the basis of the characteristics of the current available HECs, V_{ci} and V_{co} are set to 0.7 and 3.1 ms^{-1}, respectively [14,28,46,47]. These values can be adapted, if required, in forthcoming applications of the IHE index, based on future technological developments.

Fig. 5 shows the spatial distribution of E_e (top) and E_{ne} (bottom) in the Shannon Estuary. In Table 2, the mean and maximum figures of the exploitable resource in the areas identified as being of potential interest according to their available power (Areas I to VII), $E_{e,mean}$ and $E_{e,\max}$, respectively, are provided. As can be observed, the largest part of the available hydrokinetic energy in this estuary could be harnessed, as it emerges from the overall much larger figures of the exploitable rather than the non-exploitable resource. However, the difference between exploitable and non-exploitable resource largely varies throughout the estuary, being the areas with the largest exploitable energy those that present the lowest non-exploitable resource. In effect, the non-exploitable energy density in Areas I to VII is very low (<0.03 kWm^{-2}), resulting from their current velocities being higher than the cut-in of the turbines ($V_{ci} = 0.7$ ms^{-1}), throughout virtually the complete tidal cycle.

3.3. Reference energy resource and categorisation

In order to non-dimensionalise Eq. (2), and also to provide a straightforward categorisation, thus allowing simple comparisons among coastal areas and regions, the E_{ref} term is introduced in the definition of the IHE index. This term should be interpreted as a threshold value of the exploitable hydrokinetic energy resource, which is required for a feasible energy exploitation.

As a result, the dimensionless HE index constitutes a reliable metric for the quantification of the exploitable hydrokinetic energy resource at a coastal location, and it can be used as a simple way for the categorisation of its potential. Based on a thorough review of previous research on the potential of the hydrokinetic energy throughout a large number

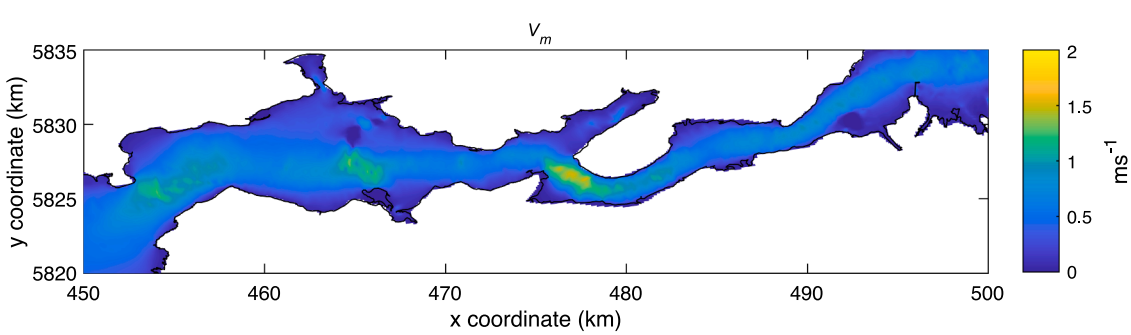

Fig. 4. Spatial distribution of V_m throughout the Shannon Estuary.

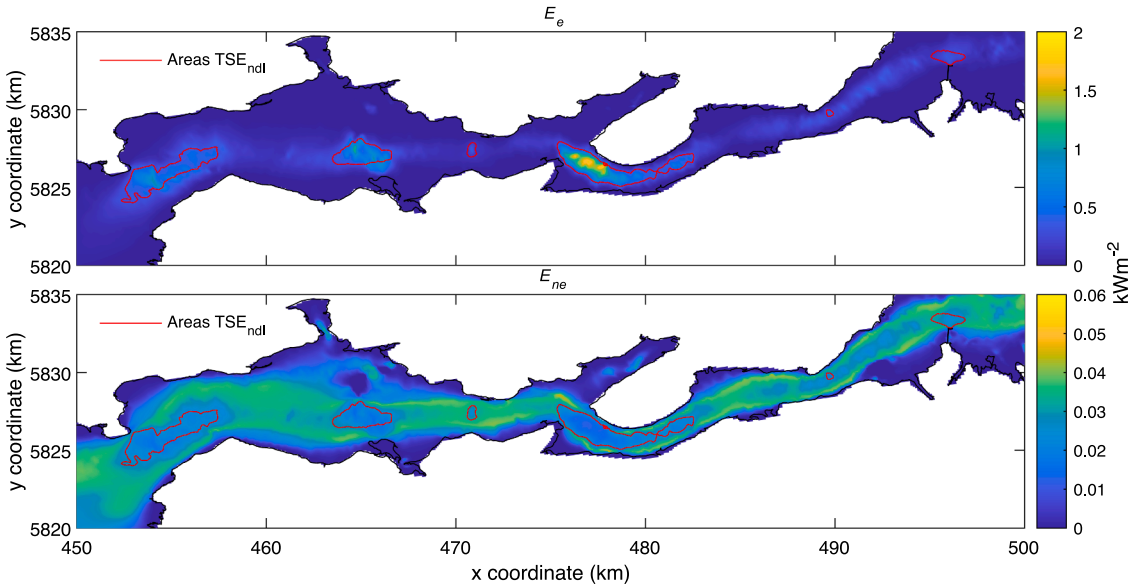

Fig. 5. Spatial distribution of E_e (top) and E_{ne} (bottom) throughout the Shannon Estuary.

Table 2
$E_{e,mean}$ and $E_{e,\max}$ in the areas of potential interest.

Area	$E_{e,mean}$ (kWm^{-2})	$E_{e,\max}$ (kWm^{-2})
I	0.47	1.02
II	0.56	1.22
III	0.21	0.41
IV	0.82	1.83
V	0.41	0.61
VI	0.37	0.44
VII	0.24	0.34

of coastal regions [10,13–15,19,20,22,25,48–53], in which current velocity data obtained by high-resolution numerical modelling and in situ measurements are analysed, the value of E_{ref} is set to 0.2 kWm^{-2}, and a total of five different categories defining the hydrokinetic energy potential are established: Zones I to V, from lower to higher potential (Table 3).

The aforementioned values can be used as a reference for any coastal region of interest, leading to a straightforward comparison with other areas; however, they could be adapted based on future technological developments. In Fig. 6, the results of the spatial distribution of the HE index throughout the Shannon Estuary are shown. The resulting mean, HE$_{mean}$, and maximum values, HE$_{max}$, of previously defined areas of interest, along with their resulting categorisation are provided in Table 4. The area with the largest exploitable resource is Area IV (HE$_{mean}$ = 3.78, category III), followed by Area II (HE$_{mean}$ = 2.58, category III) and Area I (HE$_{mean}$ = 2.16, category III) with somewhat lower resource, Area V (HE$_{mean}$ = 1.89, category II) and Area VI (HE$_{mean}$ = 1.70, category II) with significantly lower energy, and finally, Area VII (HE$_{mean}$ = 1.11, category II) and Area III (HE$_{mean}$ = 0.97, category I), which are close to the threshold of viability from a resource standpoint.

Table 3
Hydrokinetic energy resource categorization based on the HE index.

Category	HE
I	< 1
II	$1 \leq$ HE < 2
III	$2 \leq$ HE < 4
IV	$4 \leq$ HE < 8
V	≥ 8

However, these areas are extensive, presenting locations with larger values of exploitable resource and, therefore, more reduced areas could be defined for establishing a plan for hydrokinetic energy conversion.

4. Cost penalty function (C_{gp})

The next step of the methodology to implement the IHE index is the definition of a geospatial cost penalty function and its application to the Shannon Estuary. This function should relate the main drivers of CAPEX with the coastal configuration of a region, penalising the areas in which the energy exploitation will incur higher expenses, as a result of their depth and distance to the coast, but without considering a specific energy conversion technology or farm layout.

4.1. Identification of the main CAPEX drivers

CAPEX refers to the costs incurred prior to the operation of an energy installation, i.e., all the construction expenses, including the deployment and grid connection. CAPEX are usually broken down as [27,54]: (i) device costs, (ii) cable costs, (iii) foundations or mooring system costs, (iv) installation costs (e.g., transporting and deployment costs), and (v) grid connection costs. As a reference value, it can be considered that cost categories (i) to (iii) represent approx. 80% of the total CAPEX [27,55].

Device and grid connection costs are, *a priori*, independent of the geomorphology of the study area, and depend on a specific type of technology. Notwithstanding, cable and foundations, or mooring systems costs, are clearly dependent on the main geomorphological aspects, i.e., shoreline distance and water depth, respectively. Consequently, they are retained for a detailed analysis. Finally, installation costs also depend on a wide range of parameters (e.g., nautical and terrestrial transport distance, type of vessel required, climate conditions, etc.), which are difficult to evaluate accurately and, therefore, are out of the scope of this work [29].

The total (per plant) cable costs, c_c (€), can be assessed on the basis of the exporting cable cost, which allows the transport of the electric energy that is produced to a land–based electrical substation, by means of an underwater cable. As a consequence, the costs are highly influenced by the cable length and directly related to the distance to the shoreline as [27]:

$$c_c = a_2 l, \tag{7}$$

where a_2 (€m^{-1}) is an empirical coefficient which, based on [27], is

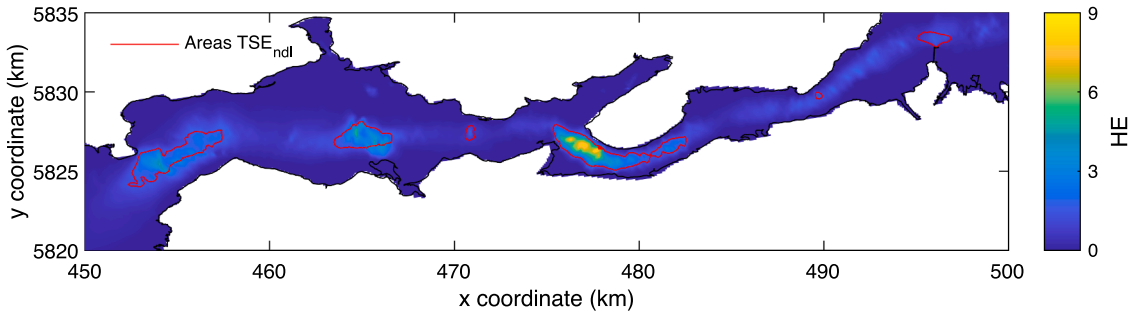

Fig. 6. Spatial distribution of the HE index throughout the Shannon Estuary.

Table 4
Categorization of areas of potential interest based on the HE index.

Area	HE_{mean}	HE_{max}	Category
I	2.16	4.70	III
II	2.58	5.62	III
III	0.97	1.89	I
IV	3.78	8.43	III
V	1.89	2.81	II
VI	1.70	2.03	II
VII	1.11	1.57	II

set as 196.96, and l (m) is the shoreline distance or, in other words, the cable length from the central hub of the hydrokinetic farm to the shoreline.

As regards the foundations, the most habitual constructive solutions are monopile gravity foundations, which are usually prescribed up to water depths of 20–30 m. Their costs, c_f (M€MW^{-1}), can be computed (per unit of converter) as a function of the water depth, h (m) as follows [27,56]:

$$c_f = 0.15 + 10^{-5}h^3. \tag{8}$$

Finally, with respect to the cost of mooring systems, c_m (€), they depend on the type of mooring solution that is used. The most habitual system is the so-called CALM (Catenary Anchor Leg Mooring) system, whose cost per energy converter is related with the mass of each mooring line, w_{CALM} (kg), by 300 € ton^{-1} as [57]:

$$c_m = 300 n_c w_{CALM}, \tag{9}$$

$$w_{CALM} = l_c d_c^2 k, \tag{10}$$

where n_c represents the number of mooring lines, l_c (m) is the length of the catenary, d_c (mm) stands for the diameter of the mooring line, which is usually set to 45 mm in the case of hydrokinetic energy devices [29]; and k (kgm^{-1}mm^{-2}) represents a constant that can be estimated as 0.02 or 0.0219 for studless and stud-link chains, respectively. Based on [57], a CALM system, which is composed by three stud–link chain lines with a total length of four times the water depth is retained. Thus, Eq. (9) can be rewritten, per unit of energy converter as:

$$c_m = 159.651h. \tag{11}$$

Regarding foundations and mooring systems, it is necessary to note that the choice between both solutions strongly depends on the specific characteristics of each energy conversion technology and, mainly, on its working principle. However, as a general rule, bottom–fixed devices usually use monopile gravity foundations when they operate up to the abovementioned water depth limit (i.e., 20–30 m); above this limit, floating devices that are anchored to the sea bottom by means of mooring lines are the most common solution [47].

What emerges from Eqs. (7) to (11), are other aspects that should be considered when assessing the influence of the coastal configuration on CAPEX, even with independence of the energy conversion technology and layout: the total plant power (Eq. (8)) and the number of devices that will compose the hydrokinetic farm so as to achieve this plant power (Eqs. (8) and (11)). For further details about these two aspects, the reader is referred to Section 4.2.

4.2. *Pre-sizing towards generalisation: Total plant power and number of devices*

The consideration of the coastal configuration in a site-selection cost-effective analysis requires, even in early project stages, a pre-sizing of a "standard" hydrokinetic farm including: (i) total power plant, and (ii) number of HECs.

There are many variables involved in defining the total plant power which may be not clear in the preliminary project stages. After a thorough analysis of the current trends and prospects of hydrokinetic technology [46] and, focusing on the hydrokinetic energy conversion in coastal regions by installing second- or third-generation converters [47], a plant with total power of 1 MW is retained.

Regarding the number of devices composing the hydrokinetic farm, the situation is similar to that in the case of the plant power; there is a vast gamut of requirements and limitations that should be considered in order to conduct a cost analysis with independence of the final layout and energy conversion technology [28,29]: available surface, area per device, security margins, etc. Similarly, there is a marked heterogeneity within hydropower projects, ranging from small-scale applications with small-sized turbines to large–scale farms, covering entire coastal regions with large-diameter turbines. Therefore, a wide range of energy conversion devices must be covered in order to generalise the results that are obtained.

Based on a thorough analysis of the current available technologies that are considered in real hydrokinetic projects [14,41,58–63], eight different types of energy converters, ranging from floating micro-turbines (Ø 1 m) to large-diameter bottom–fixed turbines (Ø 16 m), and considering representative designs, are retained (Table 5): (i) Darrieus Turbine (DT), (ii) Darrieus Ducted Turbine (DDT), (iii) Evopod Turbine (ET), (iv) Gorlov Helicoidal Turbine (GHT), (v) Smart Freestream Turbine (SFT), (vi) Smart Monofloat Turbine (SMT), (vii) SeaGen Turbine (SGT), and (viii) Savonius Turbine (ST).

The analysis of the CAPEX of a 1 MW farm, that is composed by each of these representative types of HECs, can lead to the definition of a

Table 5
Main characteristics of the HECs considered.

HEC	Diameter (m)	V_{ci} (ms^{-1})	Rated power (kW)	Swept area (m^2)
DT	1.50	0.80	1.50	2.25
DDT	1.50	0.80	2.70	3.80
ET	3.00	0.70	30.00	7.10
GHT	1.00	0.50	6.30	2.50
SFT	1.00	0.70	5.00	0.80
SMT	1.00	0.70	5.00	0.80
SGT	16.00	1.00	1200.00	400.00
ST	2.00	1.00	2.50	4.00

penalty function, C_{gp}, relating the costs and the characteristics of a given location (depth and distance to coast). The details of the development and application of this cost penalty function are presented in Section 4.3.

4.3. Development and application of the cost penalty function

The total CAPEX of a pre-sized hydrokinetic farm, as defined in Section 4.2, can be assessed by means of its total cost function, c_{farm} (€), built using Eqs. (7), 8 and 11 as:

$$c_{farm} = \begin{cases} c_c + 10^6 P n_c c_f \\ c_c + n_c c_m \end{cases} \tag{12}$$

where P (MW) represents the total plant power, and n_c is the number of converters that are required, which vary depending on the converter that is analysed. Note that the terms c_f and c_m (Eqs. (8) and (11), respectively) cannot be computed simultaneously for a given HEC, being computed based on the technical requirements of the energy converters.

Substituting each term by its value in Eq. (12), it can be rearranged as:

$$c_{farm} = \begin{cases} 196.96l + 10^6 P n_c \left[0.15 + 10^{-5} h^3\right] \\ 196.96l + n_c [159.65h] \end{cases} \tag{13}$$

This function clearly shows the relation between the estuarine coastal configuration (i.e., water depth and shoreline distance, h and l, respectively) and the total CAPEX. However, as previously stated, Eq. (13) cannot be used to represent the whole available farm configurations because of its constant coefficients (P and n_c), which must be defined. In order to generalise this function to make it representative for any hydrokinetic project, as discussed in Section 4.2, the total power plant is set to 1 MW.

However, the generalisation of this function, when considering all the different types of energy converters, is not straightforward. To this end, the values of c_{farm} for plants that are composed by the devices (i) to (viii), defined in Section 4.2, are computed and averaged. After operating and rearranging, the generalised total cost function, $c_{farm,g}$ reads:

$$c_{farm,g} = 1.5d^3 + 34624.31d + 196.96l + 22500. \tag{14}$$

Eq. (14) constitutes a generalised expression, which can be applied to any coastal area, so as to obtain an estimated assessment of CAPEX, based on the water depth and shoreline distance of a specific location. The geospatial cost penalty function, C_{gp}, can be easily obtained as:

$$C_{gp} = 1 - \frac{c_{farm,g}}{c_{farm,g,ref}}, \tag{15}$$

where $c_{farm,g,ref}$ stands for a reference value (Eq. (14)) within the coastal area of interest, or a threshold value beyond which hydrokinetic energy conversion is not feasible (corresponding to a limiting values of h and l). Based on previous analyses of hydrokinetic energy projects in coastal areas [64], $c_{farm,g,ref}$ is defined for $h = 50$ m and $l = 7.5$ km.

The representation of Eq. (15) for a generic domain up to 7.5 km distance from shoreline and 50 m water depth ($c_{farm,g,ref}$) is shown in Fig. 7. As can be observed, water depth has a more important role as CAPEX driver than shoreline distance resulting from the cubic term in Eq. (14).

The results of application of the cost penalty function, C_{gp}, to the Shannon Estuary is plotted in Fig. 8. As is apparent, the results show an excellent correlation with the coastal configuration of the estuary. In effect, values of roughly 0.4–0.6 within the central channel of the inner and middle estuary are found, approx. 0.9 in the nearest shoreline areas (virtually not penalised due to their reduced depth and distance to the coast) and plummeting to a mere 0.2 in the surroundings of the mouth (larger water depths and distance to coast). The resulting mean and maximum values of the cost penalty function, $C_{gp,mean}$, $C_{gp,\max}$, respectively, in the areas of interest (Areas I to VII) are provided in Table 6.

The area with the highest costs is Area V ($C_{gp,mean} = 0.64$), closely followed by Area I ($C_{gp,mean} = 0.67$) and Area III ($C_{gp,mean} = 0.68$), at some distance by Area II ($C_{gp,mean} = 0.71$), Area VI ($C_{gp,mean} = 0.71$) and Area IV ($C_{gp,mean} = 0.76$), and finally by Area VII ($C_{gp,mean} = 0.82$) with the lowest costs. However, as in the case of the exploitable resource analysis, and resulting from the large extension of these areas, the costs of the installation of a hydrokinetic farm significantly differ within each them, with a mean variation (mean variation between $C_{gp,mean}$ and $C_{gp,\max}$) of 24%, which in the case of Area V and Area I attains 39% and 33%, respectively. These variations may significantly alter the delimitation of the best areas for installing a hydrokinetic farm, and they have to be considered in the decision-making process.

5. Water use penalty function (U_{gp})

Coastal regions and, in particular, estuaries are usually areas of a high environmental value, which in turn produce an intense socioeconomic activity. Thus, the following step for the application of the IHE index is to assess the compatibility between hydrokinetic energy exploitation and the marine uses with which it may coexist. To this end, a water use penalty function, U_{gp}, is defined and applied to the Shannon Estuary. This function is developed as followed.

First, the marine uses and their characteristics (area occupied, intensity of the activity, etc.), taking place in a coastal region, must be identified. As was previously introduced, they can be categorised into: (i) socioeconomic activities and (ii) environmental uses. Socioeconomic

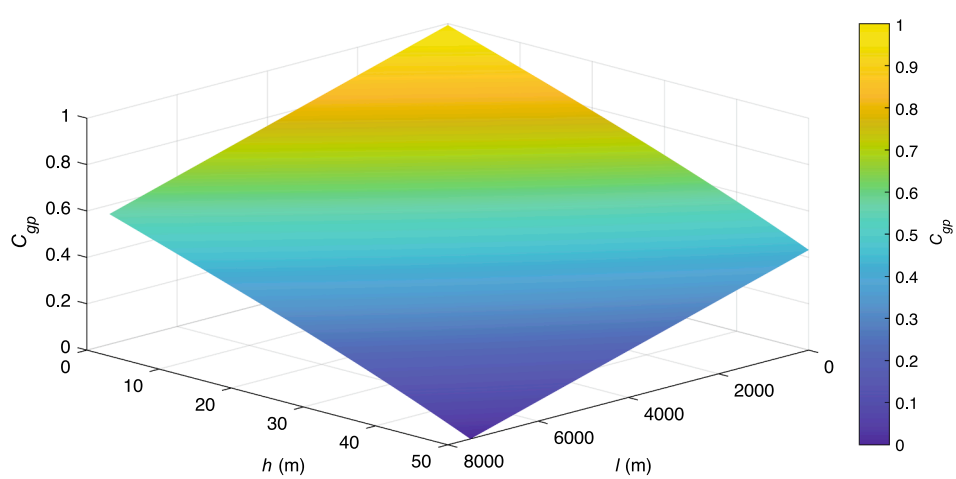

Fig. 7. Graphical representation of the geospatial cost penalty function, C_{gp} (Eq. (15)) as function of water depth, h, and shoreline distance, l.

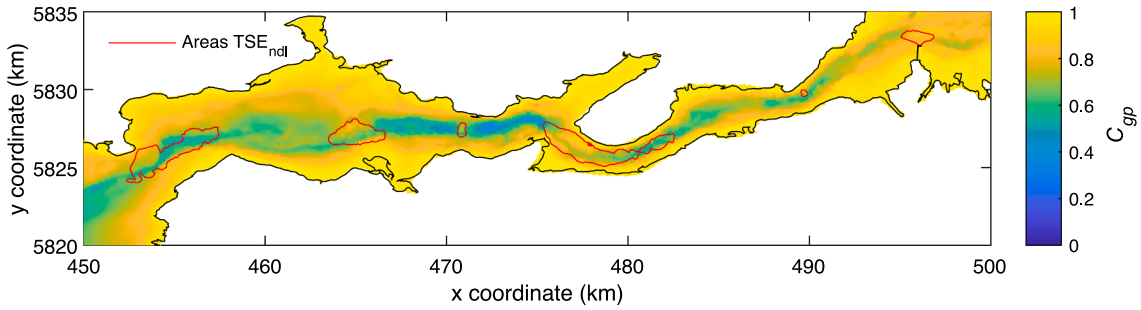

Fig. 8. Spatial distribution of C_{gp} throughout the Shannon Estuary.

Table 6
Characteristic values of C_{gp} in the areas of potential interest.

Area	$C_{gp,mean}$	$C_{gp,\max}$
I	0.67	0.89
II	0.71	0.90
III	0.68	0.73
IV	0.76	0.96
V	0.64	0.89
VI	0.71	0.81
VII	0.82	0.98

activities can be defined as those leading to a straightforward economic or social profit. On the other hand, environmental uses correspond with areas with specific characteristics that constitute the natural habitat for many different wildlife. The socioeconomic marine activities that are considered in this work are aquaculture, shellfish, and navigation. Regarding environmental uses, Special Areas of Conservation (SACs) and Special Protection Areas (SPAs) are analysed.

Next, a quantitative approach to assessing the coexistence of these marine uses, either socioeconomic or environmental, and hydrokinetic energy exploitation is proposed. The method resorts to the definition of the penalty function U_{gp} whose values range between 0 (totally restricted i.e., no coexistence) and 1 (no restrictions, i.e., full coexistence), with intermediate values that are adapted to the specific characteristics of each marine use [65], meaning a lower value of U_{gp} and a higher restriction. The values for the different types of marine uses are defined as follows.

Aquaculture farming is subclassified into extensive or intensive areas. Extensive areas represent large zones that are suitable for the installation of aquaculture farms, whereas intensive areas stand for specific existing facilities, or areas that are legally delimited for this use. Values of $U_{gp} = 0.3$ (high restriction) and $U_{gp} = 0.6$ (medium restriction) are set for intensive and extensive aquaculture farming, respectively. In the case of shellfish exploitation, it constitutes an intensive activity by definition, and therefore a value of 0.3 (high restriction) is retained with some exceptions, such as areas that are legally delimited for this use and that are, considering their particular characteristics, unsuitable for energy exploitation ($U_{gp} = 0$).

As regards navigation, it is necessary to distinguish between the presence of marine traffic of a given intensity and the delimitation of navigation channels. Both aspects are considered in this work. For the analysis of the intensity of the marine traffic, the vessel density concept, ν_d, is used, which is computed in terms of annual hours per square kilometre of water surface occupied by vessels, based on EMODnet Human Activities data [66]. After a thorough data analysis of representative European ports [67–69], a vessel density threshold of 50 hkm^{-2} is defined, meaning that areas with traffic density over this value are considered as non-suitable for energy exploitation and, therefore, penalised with a value of $U_{gp} = 0$ (totally restricted, i.e., no coexistence). Areas with traffic density figures under this threshold are considered as appropriate, but with a restriction. This restriction is computed by linearly interpolating the limits of the function ($U_{gp} = 0$ for $\nu_d = 50$ hkm^{-2} and $U_{gp} = 1$ for $\nu_d = 0$ hkm^{-2}), according to the geospatial distribution of ν_d figures. Finally, the water surface that is occupied by a navigation channel, which is legally defined, is considered as totally restricted ($U_{gp} = 0$). In the case of oversized navigation channels, these areas could be considered as partially restricted, by defining new limits according to the specific characteristics of each coastal region. With respect to the environmental uses, SACs and SPAs are assumed to be extensive areas. However, these areas occupy the whole estuary and, overall, impose a more limited restriction than in the case of an extensive economic activity (e.g., aquaculture). In these areas a value of $U_{gp} = 0.9$ (low restriction) is considered. In the case of areas with a special environmental value, in addition to SACs or SPAs, other values of U_{gp} should be considered, while attending to their specific characteristics and the resulting restrictions (medium, high, or total restriction).

Finally, in the case of the presence of various marine uses in the same area, the most restrictive value of U_{gp} is retained. Please note that the analysis of the specific impacts of hydrokinetic energy operation on the flow regime and its interactions with the surrounding water uses are out of the scope of this work, and should be analysed for each specific hydrokinetic energy project.

Fig. 9 shows the spatial distribution of the different abovementioned marine uses within the Shannon Estuary. It can be observed that extensive areas are occupied by aquaculture farming, or they are appropriate for this purpose. In addition, virtually all the extension of this estuary is used for navigation, with a legally delimited navigation area, occupying the whole main channel and various approaches to the nearby coast. Finally, environmental uses correspond, as previously stated, with areas occupying a much larger extension than the socioeconomic activity and, overall, not imposing a significant restriction for hydrokinetic energy operation. The combination of all the aforementioned uses provides a global picture of the potential available areas, and their socioeconomic and environmental restrictions for hydrokinetic energy conversion in this estuary.

A clearer understanding of the most suited areas from a socioeconomic and environmental standpoint is provided by computing the previously defined water use penalty function, U_{gp}, for the different socioeconomic and environmental uses (Fig. 10), and their combination, to obtain an overall value of U_{gp} (Fig. 11). Based on the results obtained, the extension of the areas that are identified as of interest can be significantly reduced by considering only the surface without total restriction ($U_{gp} > 0$). The resulting mean and maximum values of the

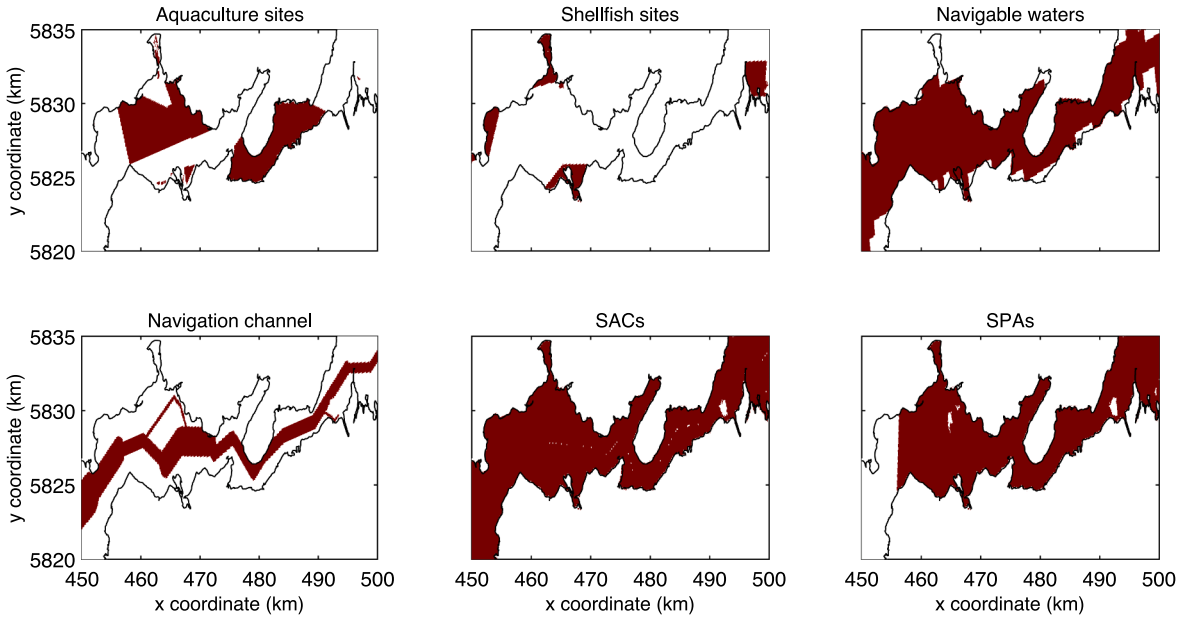

Fig. 9. Spatial distribution of marine uses (in red) within the Shannon Estuary.

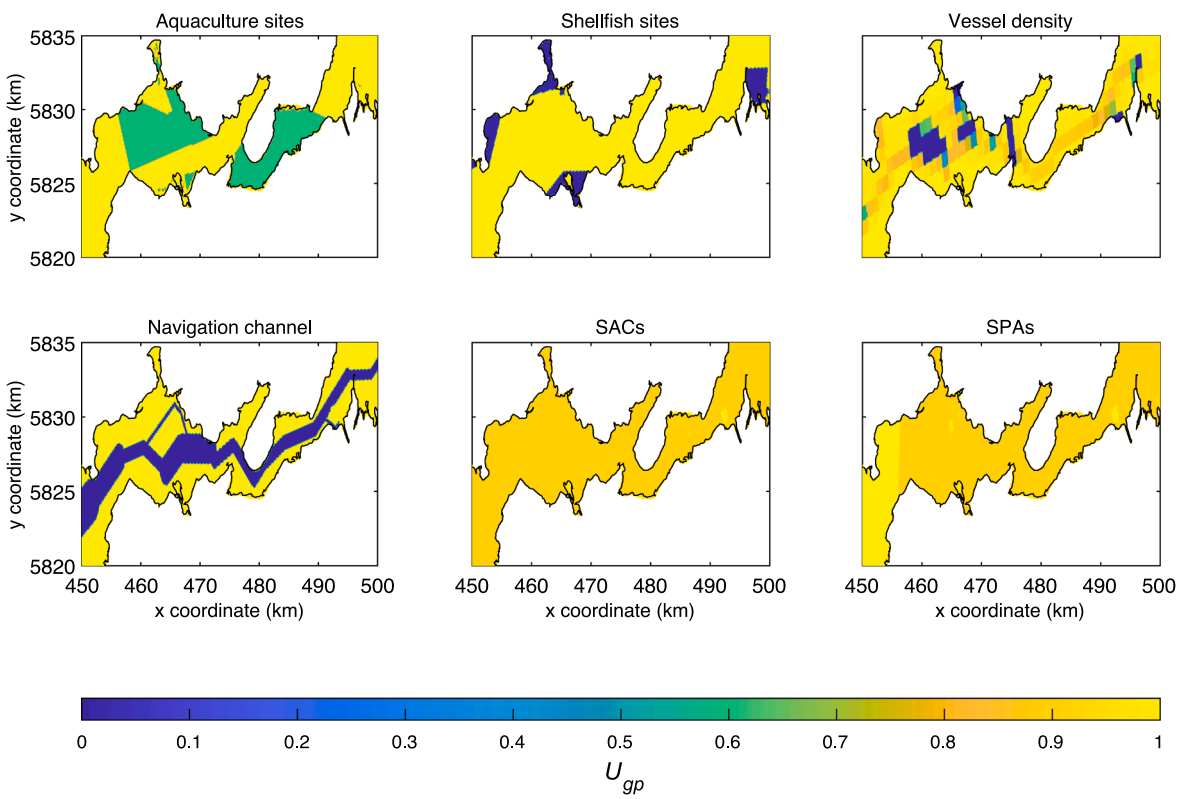

Fig. 10. Representation of U_{gp} for the different marine uses throughout the Shannon Estuary.

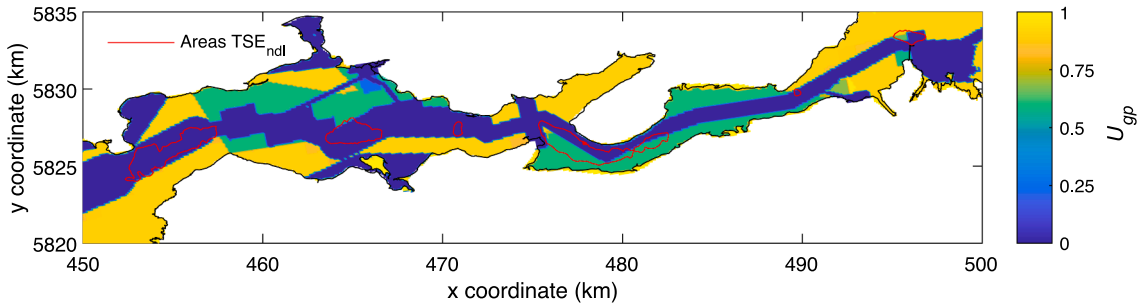

Fig. 11. Spatial distribution of U_{gp} throughout the Shannon Estuary.

Table 7
Characteristic values of U_{gp} in areas of potential interest.

Area	$U_{gp,mean}$	$U_{gp,\max}$
I ($U_{gp} > 0$)	0.88	0.90
II ($U_{gp} > 0$)	0.60	0.60
IV ($U_{gp} > 0$)	0.61	0.90
V ($U_{gp} > 0$)	0.60	0.60
VII ($U_{gp} > 0$)	0.74	0.90

penalty function, $U_{gp,mean}$ and $U_{gp,\max}$, respectively, for the new delimited surface (i.e., the surface delimited by $U_{gp} > 0$) of Areas I to VII is provided in Table 7.

The area that is compatible with hydrokinetic energy operation and presents fewer socioeconomic and environmental restrictions is Area I ($U_{gp,mean} = 0.88$), followed by Area VII ($U_{gp,mean} = 0.74$) and finally, with similar values, Area IV ($U_{gp,mean} = 0.61$), Area V ($U_{gp,mean} = 0.60$) and Area II ($U_{gp,mean} = 0.60$). Areas III and VI are not suitable for energy conversion. In contrast with the resource and costs results, the variations of U_{gp} within each area are less pronounced, with the exception of Area IV.

6. Integration of the results

The integration of the different terms considered in the proposed index leads to the geospatial distribution of the IHE index in the study region (Eq. (1)). Its physical interpretation, as was previously introduced, is straightforward: the higher the IHE index, the better the site for hydrokinetic energy exploitation, with figures above 1 indicating suitability for hydrokinetic energy exploitation. Therefore, IHE = 1 would represent a suitability threshold indicating a site with the bare minimum amount of exploitable energy (HE = 1), and without any penalisation in terms of costs derived from its coastal configuration ($C_{gp} = 1$) or from the surrounding socioeconomic or environmental uses ($U_{gp} = 1$).

Fig. 12 shows the spatial distribution of the IHE index throughout the Shannon Estuary. The areas with IHE>1 are delimited along, with the areas that are identified as of interest in previous studies (and analysed in the preceding sections). The mean and maximum values of the IHE index, IHE$_{mean}$, and IHE$_{max}$, respectively, for the new delimited areas are provided in Table 8, along with their main characteristics.

The computation of the IHE index for the Shannon Estuary allows the identification of six areas for hydrokinetic energy exploitation (Area I$_{IHE}$ to Area VI$_{IHE}$) which significantly differ from previous analyses. The most suited area is Area IV$_{IHE}$, close to Tarbert, as in the case of previous studies, but now occupying a smaller area within the previously identified Area IV, with lower available resource, and lower costs and fewer restrictions for hydrokinetic energy operation. The other newly identified areas do not correspond with those that were previously identified. Instead, the new areas are close to the previous areas, occupying a more limited surface with, again, somewhat of a lower resource, but with lower costs and fewer restrictions for energy conversion.

The results of IHE index show that Area IV$_{IHE}$ is of high interest for energy operation (IHE$_{mean}$ of category III with locations in category IV), whereas Area I$_{IHE}$, and Area III$_{IHE}$, although with less potential, are also of significant interest (IHE$_{mean}$ of category II with locations in category III). Finally, the remaining areas, Area II$_{IHE}$, Area V$_{IHE}$, and Area VI$_{IHE}$, could be of interest, but with a more limited potential (IHE$_{mean}$ close to 1).

Table 8
Characteristic values of the IHE index in new areas of interest and their main characteristics.

Area	IHE$_{mean}$	IHE$_{max}$	Surface (km^2)	Mean depth (m)	Seabed type
I$_{IHE}$	1.31	2.28	1.64	7.40	Rock
II$_{IHE,N}$	1.19	1.67	0.21	7.65	Rock
II$_{IHE,S}$	1.66	2.74	0.35	5.43	Rock
IV$_{IHE}$	2.10	4.15	2.99	16.83	Mixed sediment
V$_{IHE}$	1.04	1.28	0.28	22.73	Mixed sediment
VI$_{IHE}$	1.03	1.16	0.47	17.75	Sand

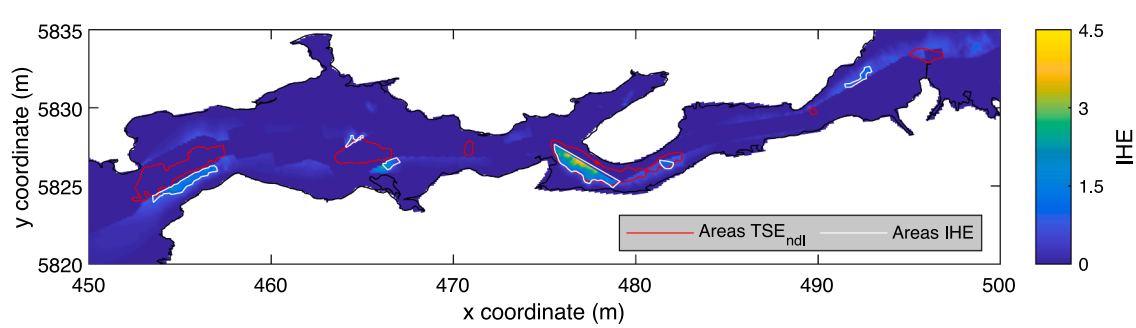

Fig. 12. Spatial distribution of the IHE index and the resulting areas of interest (Areas IHE), along with the previously identified areas (Areas TSE$_{ndl}$).

7. Conclusions

A comprehensive methodology was developed for identifying the best locations for hydrokinetic energy operation in a coastal region, The proposed methodology considers not only the resource, but also the costs of installation, along with the socioeconomic activities and environmental aspects. The combination of these aspects leads to the definition of the novel IHE index.

The methodology is composed of four steps. First, the distribution of the energy resource is investigated through the hydrokinetic energy resource index, HE index, which characterises the exploitable resource (rather than the total available resource) by considering the velocity ranges of operation of the current available HECs. Secondly, the geospatial cost penalty function, C_{gp}, is used to determine the costs of installation of a hydrokinetic farm, resulting from the coastal configuration, based on the water depth and shoreline distance. Then, the geospatial water use penalty function, U_{gp}, assesses the suitability of the coexistence of hydrokinetic energy operation with the socioeconomic activity and environmental aspects. From a resource standpoint, HE values higher than 1 indicate suitability for hydrokinetic energy operation (other restrictions are not considered at this point). Regarding the penalty functions, C_{gp} and U_{gp}, they range from 1 (no restriction) to 0 (total restriction). In the final step, the geospatial distribution of the IHE index is obtained by integrating (multiplying) the aforementioned terms (HE, C_{gp} and U_{gp}). As a result, the higher the IHE index, the better the site for hydrokinetic energy exploitation, with values above 1 indicating suitability for hydrokinetic energy exploitation. For a better interpretation of the results, different thresholds of the IHE index are established based on a thorough analysis of the available and exploitable resource in coastal regions of interest for hydrokinetic energy conversion throughout the world, leading to a total of five categories (category I to category V, from lower to higher interest).

The IHE index is applied to the Shannon Estuary to assess the potential of the areas identified in previous studies as of interest for energy conversion. A total of six areas (Area I_{IHE} to Area VI_{IHE}) are identified with an IHE index higher than 1 and, therefore, of interest for energy conversion, which differ from those selected in previous studies. The most suitable is Area IV_{IHE} (a mean IHE of category III with locations in category IV), close to Tarbert, as in the case of previous studies, but now occupying a smaller surface with somewhat lower resource and fewer restrictions for energy conversion. The remaining delimited areas do not correspond with those in previous studies.

The results show the capability of the IHE index for selecting the most appropriate locations for energy conversion in a coastal region, reducing the uncertainties in the early stages of the planning of MRE conversion. The final design of the farm configuration in subsequent stages would require a detailed cost analysis of the selected HEC-site combinations.

Declaration of Competing Interest

The authors declare that they have no known competing financial interests or personal relationships that could have appeared to influence the work reported in this paper.

Acknowledgements

This work was supported by the PORTOS project, which is co-financed by the Interreg Atlantic Area Programme, through the European Regional Development Fund [grant number EAPA_784/2018] and 'Axudas para a consolidación e estruturación de unidades de investigación competitivas nas universidades do Sistema Universitario Galego (2020-22)' with reference number ED341B 2020/25.

The authors are also grateful for the support of Science Foundation Ireland and MaREI, the Marine Renewable Energy Centre of Ireland, grant SFI MAREI2_12/RC/2302/P2 Platform RA1b.

During this work I. López was supported by a postdoctoral grant of the 'Programa de Axudas á etapa posdoutoral da Xunta de Galicia' with reference number ED481D 2019/019.

References

[1] Bhattacharya S, Pennock S, Robertson B, Hanif S, Alam MJE, Bhatnagar D, et al. Timing value of marine renewable energy resources for potential grid applications. Appl Energy 2021;299:117281.
[2] Lange M, Cummins V. Managing stakeholder perception and engagement for marine energy transitions in a decarbonising world. Renew Sustain Energy Rev 2021;152:111740.
[3] Akbari N, Jones D, Arabikhan F. Goal programming models with interval coefficients for the sustainable selection of marine renewable energy projects in the UK. Eur J Oper Res 2021;293(2):748–60.
[4] Penalba M, Aizpurua JI, Martinez-Perurena A. On the definition of a risk index based on long-term metocean data to assist in the design of Marine Renewable Energy systems. Ocean Eng 2021;242:110080.
[5] Alsaleh M, Abdul-Rahim AS. The pathway toward pollution mitigation in EU28 region: Does hydropower growth make a difference? Renewable Energy 2022;185: 291–301.
[6] Zhao Y, Xu K, Dong N, Wang H. Projection of climate change impacts on hydropower in the source region of the Yangtze River based on CMIP6. J Hydrol 2022;606:127453.
[7] Sibtain M, Li X, Bashir H, Azam MI. Hydropower exploitation for Pakistan's sustainable development: A SWOT analysis considering current situation, challenges, and prospects. Energy Strategy Reviews 2021;38:100728.
[8] Hunt JD, Nascimento A, Caten CST, Tomé FMC, Schneider PS, Thomazoni ALR, et al. Energy crisis in Brazil: Impact of hydropower reservoir level on the river flow. Energy 2022;239:121927.
[9] Zhang J, Cheng C, Yu S, Wu H, Gao M. Sharing hydropower flexibility in interconnected power systems: A case study for the China Southern power grid. Appl Energy 2021;288:116645.
[10] Carballo R, Iglesias G, Castro A. Numerical model evaluation of tidal stream energy resources in the Ría de Muros (NW Spain). Renewable Energy 2009;34(6): 1517–24.
[11] Brooks DA. The hydrokinetic power resource in a tidal estuary: The Kennebec River of the central Maine coast. Renewable Energy 2011;36(5):1492–501.
[12] Lewis M, McNaughton J, Márquez-Dominguez C, Todeschini G, Togneri M, Masters I, et al. Power variability of tidal-stream energy and implications for electricity supply. Energy 2019;183:1061–74.
[13] Fouz DM, Carballo R, López I, Iglesias G. Tidal stream energy potential in the Shannon Estuary. Renewable Energy 2022;185:61–74.
[14] Fouz DM, Carballo R, Ramos V, Iglesias G. Hydrokinetic energy exploitation under combined river and tidal flow. Renewable Energy 2019;143:558–68.
[15] Iglesias I, Bio A, Bastos L, Avilez-Valente P. Estuarine hydrodynamic patterns and hydrokinetic energy production: The Douro estuary case study. Energy 2021;222: 119972.
[16] Khojasteh D, Lewis M, Tavakoli S, Farzadkhoo M, Felder S, Iglesias G, et al. Sea level rise will change estuarine tidal energy: A review. Renew Sustain Energy Rev 2022;156:111855.
[17] Kamal MM, Saini RP. A review on modifications and performance assessment techniques in cross-flow hydrokinetic system. Sustainable Energy Technol Assess 2022;51:101933.
[18] Khan MJ, Bhuyan G, Iqbal MT, Quaicoe JE. Hydrokinetic energy conversion systems and assessment of horizontal and vertical axis turbines for river and tidal applications: A technology status review. Appl Energy 2009;86(10):1823–35.
[19] Sánchez M, Carballo R, Ramos V, Iglesias G. Energy production from tidal currents in an estuary: A comparative study of floating and bottom-fixed turbines. Energy 2014;77:802–11.
[20] Ramos V, Carballo R, Álvarez M, Sánchez M, Iglesias G. A port towards energy self-sufficiency using tidal stream power. Energy 2014;71:432–44.
[21] Iglesias G, Sánchez M, Carballo R, Fernández H. The TSE index – A new tool for selecting tidal stream sites in depth-limited regions. Renewable Energy 2012;48: 350–7.
[22] Yang Z, Wang T, Branch R, Xiao Z, Deb M. Tidal stream energy resource characterization in the Salish Sea. Renewable Energy 2021;172:188–208.
[23] Alvarez EA, Rico-Secades M, Suárez DF, Gutiérrez-Trashorras AJ, Fernández-Francos J. Obtaining energy from tidal microturbines: A practical example in the Nalón River. Appl Energy 2016;183:100–12.
[24] Mejia-Olivares CJ, Haigh ID, Wells NC, Coles DS, Lewis MJ, Neill SP. Tidal-stream energy resource characterization for the Gulf of California. México Energy 2018; 156:481–91.
[25] Robins PE, Neill SP, Lewis MJ, Ward SL. Characterising the spatial and temporal variability of the tidal-stream energy resource over the northwest European shelf seas. Appl Energy 2015;147:510–22.
[26] Vazquez A, Iglesias G. A holistic method for selecting tidal stream energy hotspots under technical, economic and functional constraints. Energy Convers Manage 2016;117:420–30.
[27] Vazquez A, Iglesias G. Capital costs in tidal stream energy projects – A spatial approach. Energy 2016;107:215–26.
[28] Lewis M, O'Hara Murray R, Fredriksson S, Maskell J, de Fockert A, Neill SP, et al. A standardised tidal-stream power curve, optimised for the global resource. Renewable Energy 2021;170:1308–23.

[29] López A, Morán JL, Núñez LR, Somolinos JA. Study of a cost model of tidal energy farms in early design phases with parametrization and numerical values. Application to a second-generation device. Renew Sustain Energy Rev 2020;117:109497.
[30] Goss ZL, Coles DS, Kramer SC, Piggott MD. Efficient economic optimisation of large-scale tidal stream arrays. Appl Energy 2021;295:116975.
[31] SIFP Steering Group. Strategic Integrated Framework Plan (SIFP) for the Shannon Estuary - An inter-jurisdictional land and marine based framework to guide the future developments and management of the Shannon Estuary. 2013.
[32] Blunden LS, Bahaj AS. Initial evaluation of tidal stream energy resources at Portland Bill. UK Renewable Energy 2006;31(2):121–32.
[33] Iglesias G, Carballo R. Effects of high winds on the circulation of the using a mixed open boundary condition: the Ría de Muros. Spain Environmental Modelling & Software 2010;25(4):455–66.
[34] Carballo R, Iglesias G, Castro A. Residual circulation in the Ría de Muros (NW Spain): A 3D numerical model study. J Mar Syst 2009;75(1-2):116–30.
[35] Iglesias G, Carballo R. Seasonality of the circulation in the Ría de Muros (NW Spain). J Mar Syst 2009;78(1):94–108.
[36] Álvarez M, Carballo R, Ramos V, Iglesias G. An integrated approach for the planning of dredging operations in estuaries. Ocean Eng 2017;140:73–83.
[37] Álvarez M, Ramos V, Carballo R, Arean N, Torres M, Iglesias G. The influence of dredging for locating a tidal stream energy farm. Renewable Energy 2020;146:242–53.
[38] Des M, deCastro M, Sousa MC, Dias JM, Gómez-Gesteira M. Hydrodynamics of river plume intrusion into an adjacent estuary: The Minho River and Ria de Vigo. J Mar Syst 2019;189:87–97.
[39] Iglesias G, Carballo R, Castro A. Baroclinic modelling and analysis of tide- and wind-induced circulation in the Ría de Muros (NW Spain). J Mar Syst 2008;74(1-2):475–84.
[40] González CJ, Reyes E, Álvarez Ó, Izquierdo A, Bruno M, Mañanes R. Surface currents and transport processes in the Strait of Gibraltar: Implications for modeling and management of pollutant spills. Ocean Coast Manage 2019;179:104869.
[41] Ramos V, Iglesias G. Performance assessment of Tidal Stream Turbines: A parametric approach. Energy Convers Manage 2013;69:49–57.
[42] Deltares. User Manual Delft3D-FLOW. Deltares ed. Delft, The Netherlands, 2010.
[43] O'Toole R, Judge M, Sacchetti F, Furey T, Mac Craith E, Sheehan K et al. Mapping Ireland's coastal, shelf and deep-water environments using illustrative case studies to highlight the impact of seabed mapping on the generation of blue knowledge. Geological Society, London, Special Publications 2020;505:SP505-2019-207.
[44] Le Provost C, Bennett AF, Cartwright DE. Ocean tides for and from Topex/Poseidon. Science 1995;267(5198):639–42.
[45] Egbert GD, Bennett AF, Foreman MGG. Topex/Poseidon tides estimated using a global inverse model. J Geophys Res 1994;99:24821–52.
[46] Chowdhury MS, Rahman KS, Selvanathan V, Nuthammachot N, Suklueng M, Mostafaeipour A, et al. Current trends and prospects of tidal energy technology. Environ Dev Sustainability 2021;23(6):8179–94.
[47] Segura E, Morales R, Somolinos JA, López A. Techno-economic challenges of tidal energy conversion systems: Current status and trends. Renew Sustain Energy Rev 2017;77:536–50.
[48] Ramos V, Ringwood JV. Implementation and evaluation of the International Electrotechnical Commission specification for tidal stream energy resource assessment: A case study. Energy Convers Manage 2016;127:66–79.
[49] Neill SP, Hashemi MR, Lewis MJ. The role of tidal asymmetry in characterizing the tidal energy resource of Orkney. Renewable Energy 2014;68:337–50.
[50] Thiébot J, Guillou S, Droniou E. Influence of the 18.6-year lunar nodal cycle on the tidal resource of the Alderney Race, France. Appl Ocean Res 2020;97:102107.
[51] O'Rourke F, Boyle F, Reynolds A. Ireland's tidal energy resource; An assessment of a site in the Bulls Mouth and the Shannon Estuary using measured data. Energy Convers Manage 2014;87:726–34.
[52] Marsh P, Penesis I, Nader JR, Cossu R, Auguste C, Osman P, et al. Tidal current resource assessment and study of turbine extraction effects in Banks Strait. Australia Renewable Energy 2021;180:1451–64.
[53] Liu X, Chen Z, Si Y, Qian P, Wu He, Cui L, et al. A review of tidal current energy resource assessment in China. Renew Sustain Energy Rev 2021;145:111012.
[54] Dalton G, Allan G, Beaumont N, Georgakaki A, Hacking N, Hooper T, et al. Economic and socio-economic assessment methods for ocean renewable energy: Public and private perspectives. Renew Sustain Energy Rev 2015;45:850–78.
[55] Allan G, Gilmartin M, McGregor P, Swales K. Levelised costs of Wave and Tidal energy in the UK: Cost competitiveness and the importance of "banded" Renewables Obligation Certificates. Energy Policy 2011;39(1):23–39.
[56] Serrano González J, Burgos Payán M, Riquelme Santos JM. An improved evolutive algorithm for large offshore wind farm optimum turbines layout. 2011 IEEE Trondheim PowerTech 2011:1–6.
[57] Astariz S, Iglesias G. Co-located wind and wave energy farms: Uniformly distributed arrays. Energy 2016;113:497–508.
[58] Tunio IA, Shah MA, Hussain T, Harijan K, Mirjat NH, Memon AH. Investigation of duct augmented system effect on the overall performance of straight blade Darrieus hydrokinetic turbine. Renewable Energy 2020;153:143–54.
[59] ed-Dín Fertahi S, Bouhal T, Rajad O, Kousksou T, Arid A, El Rhafiki T, et al. CFD performance enhancement of a low cut-in speed current Vertical Tidal Turbine through the nested hybridization of Savonius and Darrieus. Energy Convers Manage 2018;169:266–78.
[60] Marsh P, Penesis I, Nader JR, Cossu R, Auguste C, Osman P, et al. Tidal current resource assessment and study of turbine extraction effects in Banks Strait, Australia. Renewable Energy 2021;180:1451–64.
[61] Mestres M, Griñó M, Sierra JP, Mösso C. Analysis of the optimal deployment location for tidal energy converters in the mesotidal Ria de Vigo (NW Spain). Energy 2016;115:1179–87.
[62] Pudur R, Gao S. Performance Analysis of Savonius Rotor Based Hydropower Generation Scheme with Electronic Load Controller. Journal of Renewable Energy 2016;2016:1–7.
[63] Fraenkel P. Practical tidal turbine design considerations: a review of technical alternatives and key design decisions leading to the development of the SeaGen 12 MW tidal turbine 2010;19:1–19.
[64] Carballo R, López I, Areán N, Fouz DM. PORTOS Deliverable D5.6 - Technology-site selection based on high-resolution performance analysis. Universidade de Santiago de Compostela 2020.
[65] Galparsoro I, Korta M, Subirana I, Borja Á, Menchaca I, Solaun O, et al. A new framework and tool for ecological risk assessment of wave energy converters projects. Renew Sustain Energy Rev 2021;151:111539.
[66] Falco L, Pittito A, Adnams W, Earwaker N, Greidanus H. Eu Vessel density map. Detailed method 2019.
[67] Fiorini M, Capata A, Bloisi DD. AIS Data Visualization for Maritime Spatial Planning (MSP). International Journal of e-Navigation and Maritime Economy 2016;5:45–60.
[68] Vespe M, Gibin M, Alessandrini A, Natale F, Mazzarella F, Osio GC. Mapping EU fishing activities using ship tracking data. Mapping EU fishing activities using ship tracking data 2016;12(sup1):520–5.
[69] Pallotta G, Vespe M, Bryan K. Vessel Pattern Knowledge Discovery from AIS Data: A Framework for Anomaly Detection and Route Prediction. Entropy 2013;15(12):2218–45.